RSC Advances

PAPER

View Article Online
View Journal | View Issue

Cite this: *RSC Adv.*, 2023, **13**, 12065

Highly enhanced electrocatalytic OER activity of water-coordinated copper complexes: effect of lattice water and bridging ligand†

Pandi Muthukumar, [b] Gunasekaran Arunkumar, [a] Mehboobali Pannipara,[cd] Abdullah G. Al-Sehemi,[cd] Dohyun Moon *[e] and Savarimuthu Philip Anthony *[a]

The use of metal–organic compounds as electrocatalysts for water splitting reactions has gained increased attention; however, a fundamental understanding of the structural requirement for effective catalytic activity is still limited. Herein, we synthesized water-coordinated mono and bimetallic copper complexes (**CuPz-$H_2O\cdot H_2O$**, **CuPz-H_2O**, **CuBipy-$H_2O\cdot H_2O$**, and **CuMorph-H_2O**) with varied intermetallic spacing (pyrazine/4,4′-bipyridine) and explored the structure-dependent oxygen evolution reaction (OER) activity in alkaline medium. Single crystal structural studies revealed water-coordinated monometallic complexes (**CuMorph-H_2O**) and bimetallic complexes (**CuPz-$H_2O\cdot H_2O$**, **CuPz-H_2O**, **CuBipy-$H_2O\cdot H_2O$**). Further, **CuPz-$H_2O\cdot H_2O$** and **CuBipy-$H_2O\cdot H_2O$** contained lattice water along with coordinated water. Interestingly, the bimetallic copper complex with lattice water and shorter interspacing between the metal centres (**CuPz-$H_2O\cdot H_2O$**) showed strong OER activity and required an overpotential of 228 mV to produce a benchmark current density of 10 mA cm^{-2}. Bimetallic copper complex (**CuPz-H_2O**) without lattice water but the same intermetallic spacing and bimetallic complex with increased interspacing but with lattice water (**CuBipy-$H_2O\cdot H_2O$**) exhibited relatively lower OER activity. **CuPz-H_2O** and **CuBipy-$H_2O\cdot H_2O$** required an overpotential of 236 and 256 mA cm^{-2}, respectively. Monometallic **CuMorph-H_2O** showed the lowest OER activity (overpotential 271 mV) compared to bimetallic complexes. The low Tafel slope and charge transfer resistance of **CuPz-$H_2O\cdot H_2O$** facilitated faster charge transfer kinetics at the electrode surface and supported the enhanced OER activity. The chronoamperometric studies indicated good stability of the catalyst. Overall, the present structure-electrocatalytic activity studies of copper complexes might provide structural insight for designing new efficient electrocatalysts based on metal coordination compounds.

Received 22nd February 2023
Accepted 4th April 2023

DOI: 10.1039/d3ra01186k

rsc.li/rsc-advances

Introduction

Electrochemical energy conversion and energy storage technologies, such as fuel cells, metal–air batteries, and electrochemical water splitting, are receiving great attention due to the increasing concern about environmental pollution and global climate change caused by the excess burning of fossil fuels.[1,2] The electrochemical water splitting into hydrogen and oxygen offers a promising method to produce efficient, carbon-free, sustainable energy, and storage.[3–5] In particular, the electrochemical oxygen evolution reaction (OER) is an important process in all these energy conversion and storage devices.[6–8] Nevertheless, the multi-electron transfer process of OER is a thermodynamically uphill task that requires stable and efficient electrocatalysts for reducing the overpotential (η).[9,10] The precious metal-based RuO_2 and IrO_2 show excellent activity; however, their scarcity and high cost restrict their extensive practical usage.[11,12] Hence, great efforts are being made in recent years to develop earth-abundant, efficient, and low-cost OER electrocatalysts. Transition metals, especially earth-abundant 3d elements, have received great interest in developing efficient electrocatalysts due to their ability to exhibit multiple oxidation states.[13–17] Transition metal-based nanostructured materials, including oxides, oxyhydroxides, sulphides, and phosphates, homogeneous and heterogeneous metal complexes, and metal–organic frameworks (MOFs) have

[a]*School of Chemical & Biotechnology, SASTRA Deemed University, Thanjavur 613401, Tamil Nadu, India. E-mail: philip@biotech.sastra.edu*

[b]*Department of Chemistry, Saveetha School of Engineering, Saveetha Institute of Medical and Technical Sciences, Saveetha University, Chennai-600077, Tamil Nadu, India*

[c]*Research Center for Advanced Materials Science, King Khalid University, Abha 61413, Saudi Arabia*

[d]*Department of Chemistry, King Khalid University, Abha 61413, Saudi Arabia*

[e]*Beamline Department, Pohang Accelerator Laboratory, 80 Jigokro-127 Beongil, Namgu, Pohang, Gyeongbuk, Korea. E-mail: dmoon@postech.ac.kr*

† Electronic supplementary information (ESI) available: Crystal packing and electrochemical data. CCDC 2240777. For ESI and crystallographic data in CIF or other electronic format see DOI: https://doi.org/10.1039/d3ra01186k

been actively explored for developing cost-effective efficient electrocatalysts.[18–28]

Metal–organic frameworks (MOFs), which are generated by the coordination of metal ions and organic ligands, have emerged as an important class of porous materials in catalysis/electrocatalysis because of their tunable porosity, large surface area, and tailorable structures and functionality.[29–38] However, the bulky organic linkers reduce the electric conductivity of MOFs as well as hinder the accessibility to the active metal sites that often contribute to the low electrocatalytic activity. To improve the conductivity, composites of MOFs are made by combining them with conducting graphene oxide or acetylene black.[39] The use of π-conjugated dithiolene ligands showed improvement in coordination polymer conductivity and electrocatalytic activity.[40–44] The coordination environment and functionality of ligands can strongly influence the activity of MOFs. For instance, two Co-MOFs with similar coordination modes showed drastically different electrocatalytic activity due to variations in water coordination.[45] Water-coordinated Cu-peptoid complex exhibited enhanced water oxidation in the borate buffer medium.[46] Recently, we have observed a strong enhancement of copper coordination in the electrocatalytic activity polymers by coordinated water molecules and hydrophilic functionalities.[47–49] The interlinking of metal active centres in coordination polymer and increasing conjugation strongly enhanced the electrocatalytic activity compared to the complex with a similar coordination environment.[47–51] However, still it is a challenge to design the structure of new coordination complexes/polymers/MOFs with enhanced electrocatalytic activity and required more systematic studies with a series of complexes/polymers.

In continuation of our previous works on copper coordination complex/polymer designing and fabricating electrocatalysts,[42–44] herein, we have prepared a series of water-coordinated copper complexes (Scheme 1) with different spacers and investigated the electrocatalytic OER activity in an alkaline medium. Single crystal structural studies confirmed water-coordinated mono and bimetallic copper complexes, the inclusion of lattice water with varied interspacing. Interestingly, water-coordinated copper complexes along with lattice water (**CuPz-$H_2O\cdot H_2O$**) showed stronger OER activity (required 228 mV to produce 10 mA cm^{-2} current density) compared to only water-coordinated complex (**CuPz-$H_2O\cdot H_2O$** required 236 mV to produce 10 mA cm^{-2} current density). Further, the bimetallic complex connected with a shorter spacer showed higher activity compared to the longer spacer (228 *vs.* 256 mV to produce 10 mA cm^{-2} current density). The bimetallic copper complexes showed stronger activity compared to the mononuclear complex with water coordination.

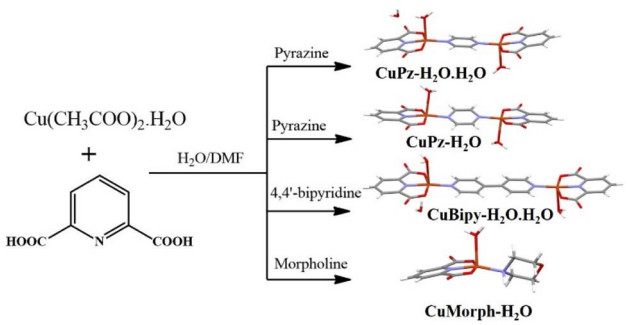

Scheme 1 Synthesis of water-coordinated mono and bimetallic copper complexes.

Experimental

Copper nitrate trihydrate ($Cu(NO_3)_2\cdot 3H_2O$), pyridine dicarboxylic acid, pyrazine, 4,4′-bipyridine, and morpholine were purchased from Sigma-Aldrich India and used as received. Nafion (product number: 274704), 5 wt% in lower aliphatic alcohols and water containing 15–20% water was obtained from Sigma-Aldrich. Carbon cloth (CC) was purchased from the electrode store in Tamil Nadu, India.

Synthesis of CuPz-$H_2O\cdot H_2O$, CuPz-H_2O, CuBipy-$H_2O\cdot H_2O$, and CuMorph-H_2O[49,52]

CuPz-$H_2O\cdot H_2O$, CuBipy-$H_2O\cdot H_2O$ and CuMorph-H_2O. $Cu(NO_3)_2\cdot 3H_2O$ (0.3 mM, 0.074 g), PDC (0.4 mM, 0.068 g) and pyrazine (0.45 mM, 0.038 g) were dissolved in 15 ml water and sonicated for 20 min to form a clear solution. The final mixture was taken in a Teflon-lined stainless-steel autoclave and was heated in an oven at 120 °C for 36 hours, then cooled to room temperature. The blue crystals of **CuPz-$H_2O\cdot H_2O$** (yield = 70%, 0.077 g) were collected (Fig. S1†), washed with DMF, and dried under a vacuum. In the same synthetic methods, 4,4′-bipyridine (0.067 g) and morpholine (37 μl) were used instead of pyrazine that produced **CuBipy-$H_2O\cdot H_2O$** (yield = 72%, 0.086 g) and **CuMorph-H_2O** (yield = 76%, 0.091 g), respectively.

CuPz-H_2O.[53] In a similar experiment to **CuPz-$H_2O\cdot H_2O$**, DMF was used in place of water as a solvent to form **CuPz-H_2O** crystals (yield = 72%, 0.072 g, Fig. S1†).

Characterization

FT-IR was measured on a PerkinElmer Spectrum 3 FT-IR spectrometer (L1280127). The phase and the crystallographic structure were identified using X-ray diffraction (XRD, Brucker, Cu-Kα: $\lambda = 0.1540598$ nm) at a scanning rate of 0.07° s^{-1} with 2θ ranging from 10° to 80°. Single crystals were coated with paratone-N oil and the diffraction data were measured using the synchrotron radiation ($\lambda = 0.62998$ Å) on an ADSC Quantum-210 detector at 2D SMC with a silicon (111) double crystal monochromator (DCM) at the Pohang Accelerator Laboratory, Korea. The crystallographic data from this paper is with the Cambridge crystallographic data centre (CCDC) no. 2240777. Thermogravimetric analysis (TGA) was performed using PerkinElmer TGA-8000 at N_2 atmosphere. X-ray photoelectron spectroscopic (XPS) analysis was performed using a K-Alpha instrument (XPS KAlpha surface analysis, Thermo Fisher Scientific, UK).

Electrochemical measurements

The electrochemical measurements were performed using a three-electrode configuration (electrochemical work station -

CHI660E, Austin, Texas, USA) with modified carbon cloth (CC) as the working electrode, graphite rod as a counter electrode, and Hg/HgO as a reference electrode in 1.0 M KOH electrolyte solution. Carbon cloth was pre-treated with HNO_3 and ethanol for 30 minutes to increase the hydrophilic nature. 4 mg of the catalyst was dispersed in 125 μl water, 125 μl ethanol, and 50 μl Nafion, and sonicated for 20 minutes to form a homogenous dispersion. 4 μl dispersed solution was drop cast onto the carbon cloth. Using the same electrodes, linear sweep voltammetry (LSV) was performed at a scan rate of 1 mV s^{-1}. For the stability studies, 1000 cycles of CV cycling were performed at 100 mV s^{-1}. All the potentials were converted to the reversible hydrogen electrode (RHE) according to the following equation: $E_{RHE} = E_{SCE} + E^{\circ}_{SCE} + (0.059\ pH)$. Electrochemical impedance spectroscopy (EIS) was performed (270 mV) with frequencies of 0.1 to 1 000 000 Hz and 10 mV amplitude in 1.0 M KOH solution. The non-faradaic region was investigated using cyclic voltammetry at various scan rates (10–100 mV s^{-1}) to quantify the electrochemical surface area.

Results and discussion

Cu^{2+} was chosen to synthesise metal coordination compounds because of its versatile coordination geometry and the possibility of obtaining the water-coordinated complex/polymer.[44–46] Similarly, pyridine dicarboxylic acid (PDA) ligands can exhibit varied coordination modes depending on the experimental condition.[44] The mixing of Cu^{2+}, PDA, and pyrazine (Pz)/bipyridine (Bipy)/morpholine (Morph) at a 1 : 1 : 1 ratio in water/DMF produced bimetallic copper complexes with different spacers (Pz/Bipy) and a mononuclear copper complex. The solid-state structural analysis confirmed the water coordination with the Cu metal centre in all four complexes (Fig. 1). Apart from water coordination, an additional water molecule was also present in the lattice of **CuPz-H_2O·H_2O** and **CuBipy-H_2O·H_2O**. Only coordinated water molecules are present in **CuPz-H_2O** and **CuMorph-H_2O**. It is noted that the single crystal structure **CuPz-H_2O·H_2O**, **CuPz-H_2O**, and **CuBipy-H_2O·H_2O** are perfectly matched with the reported copper complex.[49,52,53] The copper ions displayed distorted square-pyramidal geometry in all complexes. In **CuPz-H_2O·H_2O**, pyrazine and PDA aromatic rings displayed coplanar conformation while pyrazine adopted slightly twisted conformation in **CuPz-H_2O** (Fig. 1). Similarly, the bipyridine and PDA rings displayed a coplanar conformation in **CuBipy-H_2O·H_2O** (Fig. 1). Thus, the inclusion of lattice water forced a coplanar conformation between the aromatic amine and PDA ligand.

The lattice water solvent involved in intermolecular H-bonding with coordinated water and the carbonyl oxygen of another molecule that connected the molecules in the crystal lattice of **CuPz-H_2O·H_2O** (Fig. 2). The intermolecular H-bonding was between the coordinated water and coordinated carbonyl oxygen interconnected the molecules in **CuPz-H_2O** and **CuMorph-H_2O** (Fig. 2). The molecules in the crystal lattice of **CuBipy-H_2O·H_2O** are interconnected by H-bonding of lattice water as well as coordinated water with another molecule (Fig. 2). The intermolecular H-bonding of interactions of lattice water and coordinated water in the crystal lattice of **CuPz-H_2O·H_2O** and **CuBipy-H_2O·H_2O** produced a 3D network structure (Fig. S2 and S4†). However, the coordinated water molecule H-bonding interaction in the crystal lattice of **CuPz-H_2O** and **CuMorph-H_2O** produced a 2D network structure (Fig. 2, S3, and S5†). PXRD studies were performed to confirm the phase purity of the samples. The perfect matching between the simulated and experimental PXRD pattern confirmed the phase purity of the samples (Fig. 3). The presence of the coordinated and non-coordinated water molecules in the complexes was further confirmed by thermogravimetric analysis (TGA, Fig. 4). **CuPz-H_2O·H_2O** and **CuBipy-H_2O·H_2O** showed weight loss from 50 °C

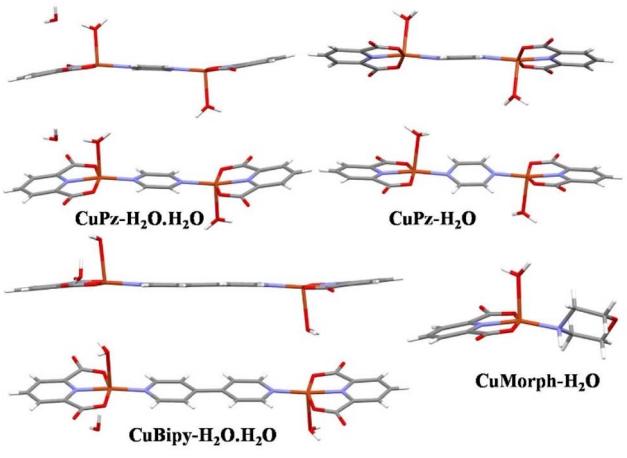

Fig. 1 Molecular structure and conformation of copper complexes in the crystal lattice of **CuPz-H_2O·H_2O**, **CuPz-H_2O**, **CuBipy-H_2O·H_2O**, and **CuMorph-H_2O**. C (grey), H (white), N (blue), O (red), and Cu (brown).

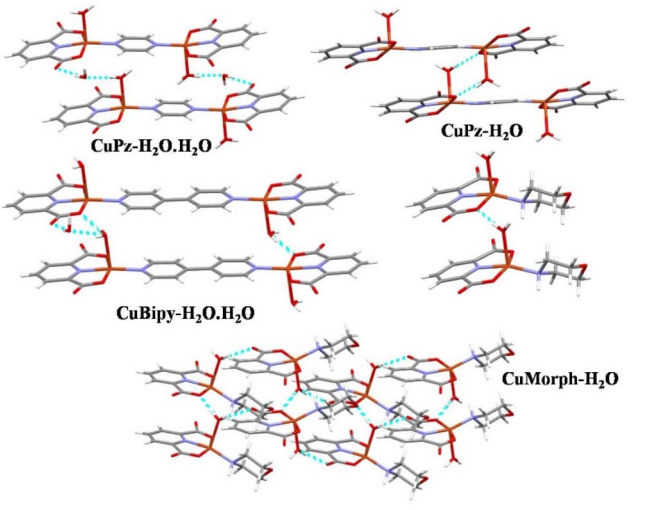

Fig. 2 Intramolecular H-bonding interactions in the crystal lattice **CuPz-H_2O·H_2O**, **CuPz-H_2O**, **CuBipy-H_2O·H_2O**, and **CuMorph-H_2O**. C (grey), H (white), N (blue), O (red), and Cu (brown). The dotted lines indicate the hydrogen bonding interactions. H-bond distances ranged between 2.733 and 2.980 Å.

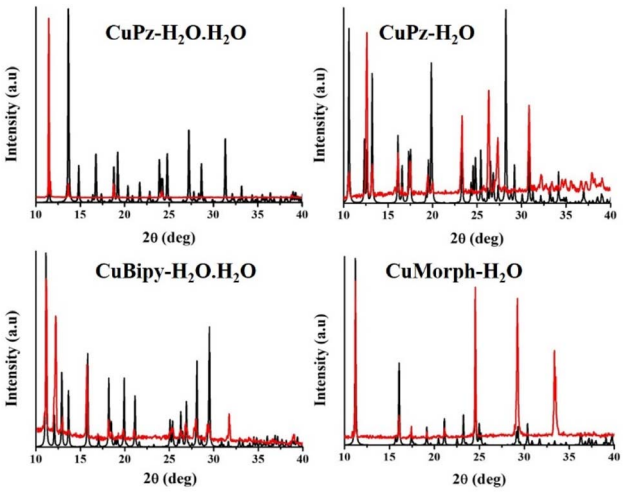

Fig. 3 Comparison of simulated (black line) and experimental (red line) PXRD pattern of copper complexes.

onwards due to the removal of lattice water molecules. However, the coordinated water molecule in **CuPz-H_2O** and **CuMorph-H_2O** was removed only after 120 °C. All four complexes decomposed around 300 °C. FTIR also further confirmed the water coordination by exhibiting a broad peak around 3500 cm^{-1} (Fig. S6†).

The electrocatalytic OER studies for copper complex catalysts coated on carbon cloth (CC) were performed using linear sweep voltammetry (LSV) in a standard three-electrode cell in 1.0 M alkaline medium (pH = 14.0) at a scan rate of 1 mV s^{-1}. In the same condition, electrochemical measurements were also performed for the bare CC electrode and commercial RuO_2 for comparison. As expected, the bare CC electrode did not show any significant OER activity (Fig. 5a). However, the copper complexes modified CC electrode showed highly enhanced but varied OER activity depending upon the complex. **CuPz-$H_2O\cdot H_2O$** exhibited a comparatively higher electrocatalytic

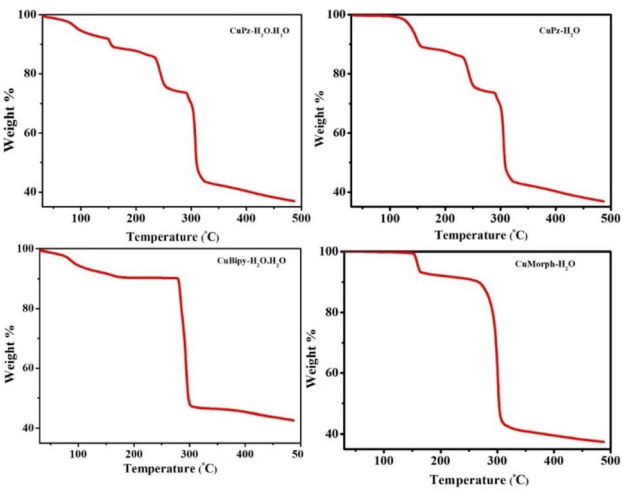

Fig. 4 TG analysis of the copper complexes.

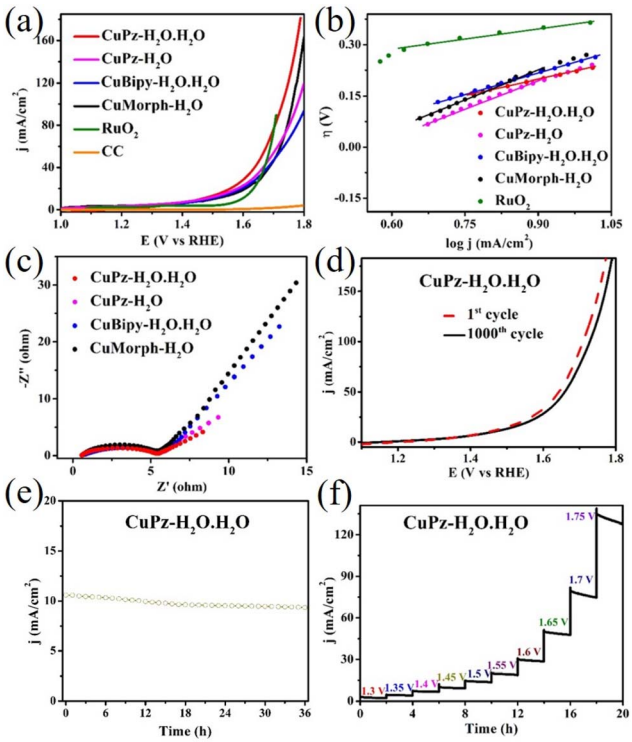

Fig. 5 (a) OER polarization curves (scan rate 1 mV s^{-1}), (b) Tafel plots of copper complexes, (c) electrochemical impedance spectra of copper complexes, and (d–f) stability studies of **CuPz-$H_2O\cdot H_2O$**. (d) OER curve of **CuPz-$H_2O\cdot H_2O$** at the 1st cycle (before OER) and after 1000th cycles showed the same activity, (e) current–time amperometric test and (f) multi-potential step studies of **CuPz-$H_2O\cdot H_2O$**.

activity among the copper complexes (Fig. 5a and S7†). **CuPz-$H_2O\cdot H_2O$** required an overpotential of 228 mV to produce a benchmark current density of 10 mA cm^{-2}. **CuPz-H_2O**, **CuBipy-$H_2O\cdot H_2O$**, and **CuMorph-H_2O** required the overpotential of 236, 256, and 271 mV for achieving 10 mA cm^{-2} current density. The commercial RuO_2 fabricated CC electrode required 364 mV for producing the current density of 10 mA cm^{-2}. **CuPz-$H_2O\cdot H_2O$** also exhibited the highest current density (175.2 mA cm^{-2}) compared to other copper complexes at the applied potential. Tafel slope analysis showed the lowest value for **CuPz-$H_2O\cdot H_2O$** (55.8 mV dec^{-1}) compared to bimetallic **CuPz-H_2O** (57.5 mV dec^{-1}) and **CuBipy-$H_2O\cdot H_2O$** (63.2 mV dec^{-1}) as well as monometallic **CuMorph-H_2O** (71.8 mV dec^{-1}, Fig. 5b). RuO_2 showed a Tafel slope of 67 mV dec^{-1}. The low Tafel value of **CuPz-$H_2O\cdot H_2O$** suggested faster kinetics compared to other copper complexes. The electrochemical impedance (EIS) measurement also showed relatively low charge transfer resistance for the **CuPz-$H_2O\cdot H_2O$** complex compared to other complexes as well as commercial RuO_2 (Fig. 5c). **CuPz-$H_2O\cdot H_2O$** showed charge transfer resistance of 5.28 Ω whereas **CuPz-H_2O**, **CuBipy-$H_2O\cdot H_2O$**, and **CuMorph-H_2O** exhibited charge transfer resistances of 6.03, 17.41, and 19.87 Ω, respectively. The low charge transfer resistance of **CuPz-$H_2O\cdot H_2O$** further supported the stronger OER catalytic activity compared to other complexes. The comparison of LSV

curves of **CuPz-$H_2O\cdot H_2O$** electrode between the 1st and 1000th cycle showed negligible variation and indicated the good stability of the catalysts (Fig. 5d). The current–time amperometric test was performed for **CuPz-$H_2O\cdot H_2O$** at the overpotential of 228 mV (1.0 M KOH, a current density of 10 mA cm^{-2} and room temperature) showed only slight decrease of current density in 36 h and suggested good stability of the catalyst (Fig. 5e). The current–time amperometric studies at higher potential and current density (380 mV and 30 mA cm^{-2}) also displayed good stability over 30 h (Fig. S8†). The current–time amperometric test was also performed by step-wise increasing the potential and observing the current density using the **CuPz-$H_2O\cdot H_2O$** catalyst (Fig. 5f). At the low applied potential, the **CuPz-$H_2O\cdot H_2O$** catalyst showed constant current density; however, it showed a decrease of current density at a higher applied potential. Further, XPS analysis of **CuPz-$H_2O\cdot H_2O$** suggested that copper is present in a +2 oxidation state with a similar electronic environment as that in the as-prepared formed, after pasting onto the carbon cloth and after electrocatalysis (Fig. S9†). High-resolution XPS spectra of Cu (as-prepared and after pasting onto carbon cloth) showed peaks at 934.65 and 954.48 eV, corresponding to Cu $2p_{3/2}$ and Cu $2p_{1/2}$, respectively. After electrochemical studies, Cu $2p_{3/2}$ and Cu $2p_{1/2}$ peaks were observed at 933.74 and 953.67 eV, respectively.

The electrochemical double layer capacitance (C_{dl}) of the catalyst provided insights into the OER activity of the catalysts. The electrochemical double layer capacitance for **CuPz-$H_2O\cdot H_2O$**, **CuPz-H_2O**, **CuBipy-$H_2O\cdot H_2O$**, and **CuMorph-H_2O** was calculated based on linear proportionality. The non-faradaic region of **CuPz-$H_2O\cdot H_2O$**, **CuPz-H_2O**, **CuBipy-$H_2O\cdot H_2O$**, and **CuMorph-H_2O** are shown in Fig. S10.† The slopes obtained from the linear relationship of the current density differences ($J_{anode} - J_{cathode}$) *vs.* the scan rate indicated high active sites in **CuPz-$H_2O\cdot H_2O$** compared to those in the other complexes (Fig. 6). **CuPz-$H_2O\cdot H_2O$** exhibited slightly higher C_{dl} (3.3 mF cm^{-2}) compared to **CuPz-H_2O** (C_{dl} = 3.1 mF cm^{-2}), **CuBipy-$H_2O\cdot H_2O$** (C_{dl} = 2.8 mF cm^{-2}), and **CuMorph-H_2O** (C_{dl} = 2.4 mF cm^{-2}).

The comparison of the copper complexes structure with OER activity showed a very interesting trend in the OER activity. Monometallic complex, **CuMorph-$H_2O\cdot H_2O$** exhibited the lowest activity compared to bimetallic copper complexes and indicated that interconnected metal active centres could be beneficial for enhancing activity.[44–46] Among the bimetallic copper complexes, **CuPz-$H_2O\cdot H_2O$** and **CuPz-H_2O** displayed similar coordination except for the presence of lattice water molecules in the former. But the higher activity of **CuPz-$H_2O\cdot H_2O$** suggested that the presence of lattice water along with coordinated water might help improve the activity. Both **CuPz-$H_2O\cdot H_2O$** and **CuBipy-$H_2O\cdot H_2O$** showed similar coordination geometry, water coordination, and lattice water. However, the metal centres in **CuPz-$H_2O\cdot H_2O$** are connected using a shorter linker, pyrazine whereas metal centres are connected by a longer spacer, 4,4′-bipyridine in **CuBipy-$H_2O\cdot H_2O$**. Interestingly, **CuPz-$H_2O\cdot H_2O$** showed stronger OER activity compared to **CuBipy-$H_2O\cdot H_2O$**. Thus, the interconnected active metal centres separated by shorter distances might have better electronic coupling and improved electrocatalytic activity.

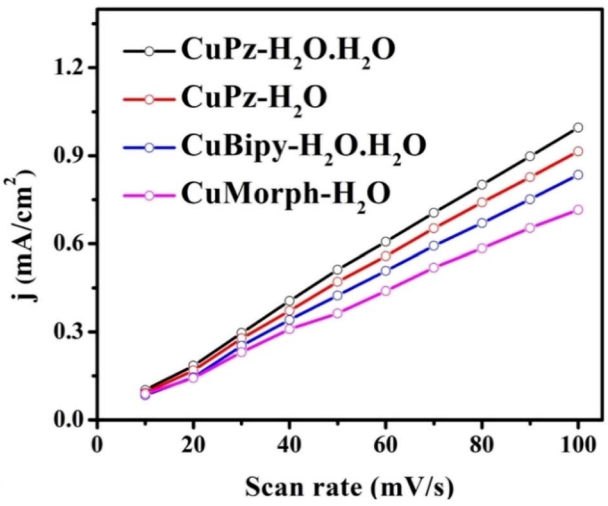

Fig. 6 Double layer capacitance and capacitive currents as a function of the scan rate.

Conclusion

In summary, water-coordinated mono and bimetallic copper coordination complexes with similar coordination environments were synthesized and compared for the structure-dependent OER activity in an alkaline medium. **CuMorph-H_2O** formed as monometallic water coordinated complex whereas **CuPz-$H_2O\cdot H_2O$**, **CuPz-H_2O**, and **CuBipy-$H_2O\cdot H_2O$** formed bimetallic water coordinated complex with different interspacing between the metal centre. OER studies of **CuMorph-H_2O** showed the lowest activity that required 271 mV to produce 10 mA cm^{-2} current density. Interestingly, the bimetallic complexes showed enhanced OER activity. The presence of lattice water with short interspacing between the metal centre in **CuPz-$H_2O\cdot H_2O$** produced strong OER activity. It required an overpotential of 226 mV to achieve the 10 mA cm^{-2} current density. The complex without the lattice water (**CuPz-H_2O**) and with lattice water but increased interspacing (**CuBipy-$H_2O\cdot H_2O$**) exhibited relatively low OER activity. **CuPz-H_2O** and **CuBipy-$H_2O\cdot H_2O$** required an overpotential of 236 and 256 mV to produce 10 mA cm^{-2} current density, respectively. Tafel slope analysis and impedance studies suggested faster reaction kinetics with low charge transfer resistance in **CuPz-$H_2O\cdot H_2O$** and supported the enhanced OER activity. **CuPz-$H_2O\cdot H_2O$** also exhibited good stability over 36 h. Thus, the present studies indicated that interconnected metal active centres with short intermetallic distances in metal coordination compounds might facilitate better electronic coupling and promote the electrocatalytic activity.

Conflicts of interest

There are no conflicts to declare.

Acknowledgements

Financial support from the Science and Engineering Research Board (SERB), Core Research grant (CRG) (CRG/2020/003978) New Delhi, India is acknowledged with gratitude. The Deanship of scientific research at King Khalid University is greatly appreciated for funding (R.G.P.1/274/43). The X-ray crystallography was supported by Basic Science Research Program through the National Research Foundation of Korea (NRF) funded by the Ministry of Education, Science, and Technology (NRF-2021R1A2C1003080).

References

1 S. Chu, Y. Cui and N. Liu, *Nat. Mater.*, 2017, **16**, 16–22.
2 E. Hu, X.-Y. Yu, F. Chen, Y. Wu and X. W. Lou, *Adv. Energy Mater.*, 2018, **9**, 1702476.
3 Z. Zhou, X. Li, Q. Li, Y. Zhao and H. Pang, *Mater. Today Chem.*, 2019, **11**, 169–196.
4 H. Sun, Z. Yan, F. Liu, W. Xu, F. Cheng and J. Chen, *Adv. Mater.*, 2020, **32**, 1806326.
5 B. Zhang, Y. Zheng, T. Ma, C. Yang, Y. Peng, Z. Zhou, M. Zhou, S. Li, Y. Wang and C. Cheng, *Adv. Mater.*, 2021, **33**, 2006042.
6 Y. Jiao, Y. Zheng, M. Jaroniec and S. Z. Qiao, *Chem. Soc. Rev.*, 2015, **44**, 2060.
7 R. P. Putra, H. Horino and I. I. Rzeznicka, *Catalysts*, 2020, **10**, 233.
8 P. P. Wang, J. An, Z. Ye, W. Cai and X. Zheng, *Front. Chem.*, 2022, **10**, 913874.
9 C. Tang, N. Cheng, Z. Pu, W. Xing and X. Sun, *Angew. Chem., Int. Ed.*, 2015, **54**, 9351–9487.
10 C. C. L. McCrory, S. Jung, I. M. Ferrer, S. Chatman, J. C. Peters and T. F. Jaramillo, *J. Am. Chem. Soc.*, 2015, **137**, 4347–4357.
11 H. Guo, Z. Fang, H. Li, D. Fernandez, G. Henkelman, S. M. Humphrey and G. Yu, *ACS Nano*, 2019, **13**, 13225–13234.
12 Y. Xing, J. Ku, W. Fu, L. Wang and H. Chen, *Chem. Eng. J.*, 2020, **395**, 125149.
13 F. Song, L. Bai, A. Moysiadou, S. Lee, C. Hu, L. Liardet and X. Hu, *J. Am. Chem. Soc.*, 2018, **140**, 7748–7759.
14 K. Wang, X. Wang, Z. Li, B. Yang, M. Ling, X. Gao, J. Lu, Q. Shi, L. Lei, G. Wu and Y. Hou, *Nano Energy*, 2020, **77**, 105162.
15 K. Zhang and R. Zou, *Small*, 2021, **17**, 2100129.
16 W. Shao, M. Xiao, C. Yang, M. Cheng, S. Cao, C. He, M. Zhou, T. Ma, C. Cheng and S. Li, *Small*, 2022, **18**, 2105763.
17 S. Sanati, A. Morsali and H. García, *Energy Environ. Sci.*, 2022, **15**, 3119–3151.
18 T. N. Huan, G. Rousse, S. Zanna, I. T. Lucas, X. Xu, N. Menguy, V. Mougel and M. Fontecave, *Angew. Chem., Int. Ed.*, 2017, **56**, 4792–4796.
19 Z. Wang, Y. Wang, N. Zhang, L. Ma, J. Sun, C. Yu, S. Liu and R. Jiang, *J. Mater. Chem. A*, 2022, **10**, 10342–10349.
20 J. Kundu, S. Khilari, K. Bhuniaa and D. Pradhan, *Catal. Sci. Technol.*, 2019, **9**, 406–417.
21 S. M. Pawar, B. S. Pawar, P. T. Babar, A. T. A. Ahmed, H. S. Chavan, Y. Jo, S. Cho, J. Kim, A. I. Inamdar, J. H. Kim, H. Kim and H. Im, *Mater. Lett.*, 2019, **241**, 243–247.
22 W. Ahn, M. G. Park, D. U. Lee, M. H. Seo, G. Jiang, Z. P. Cano, F. M. Hassan and Z. Chen, *Adv. Funct. Mater.*, 2018, **28**, 1802129.
23 X. Wang, W. Zhou, Y.-P. Wu, J.-W. Tian, X.-K. Wang, D.-D. Huang, J. Zhao and D.-S. Li, *J. Alloys Compd.*, 2018, **753**, 228–233.
24 J. He, F. Liu, Y. Chen, X. Liu, X. Zhang, L. Zhao, B. Chang, J. Wang, H. Liu and W. Zhou, *Chem. Eng. J.*, 2022, **432**, 134331.
25 H. Yuan, L. Zhao, B. Chang, Y. Chen, T. Dong, J. He, D. Jiang, W. Yu, H. Liu and W. Zhou, *Appl. Catal., B*, 2022, **314**, 121455.
26 B. Singh, A. Yadava and A. Indra, *J. Mater. Chem. A*, 2022, **10**, 3843–3868.
27 N. Seal, K. Karthick, M. Singh, S. Kundu and S. Neogi, *Chem. Eng. J.*, 2022, **429**, 132301.
28 S. Sanati, A. Morsali and H. García, *Energy Environ. Sci.*, 2022, **15**, 3119–3151.
29 I. Hod, P. Deria, W. Bury, J. E. Mondloch, C.-W. Kung, M. So, M. D. Sampson, A. W. Peters, C. P. Kubiak, O. K. Farha and J. T. Hupp, *Nat. Commun.*, 2015, **6**, 8304.
30 E. M. Miner, T. Fukushima, D. Sheberla, L. Sun, Y. Surendranath and M. Dincă, *Nat. Commun.*, 2016, **7**, 10942.
31 Y.-B. Huang, J. Liang, X.-S. Wang and R. Cao, *Chem. Soc. Rev.*, 2017, **46**, 126–157.
32 Q. Yang, Q. Xu and H.-L. Jiang, *Chem. Soc. Rev.*, 2017, **46**, 4774–4808.
33 T. Drake, P. Ji and W. Lin, *Acc. Chem. Res.*, 2018, **51**, 2129–2138.
34 X. Su, Y. Wang, J. Zhou, S. Gu, J. Li and S. Zhang, *J. Am. Chem. Soc.*, 2018, **140**, 11286–11292.
35 C.-D. Wu and M. Zhao, *Adv. Mater.*, 2017, **29**, 1605446.
36 D.-H. He, J. J. Liu, Y. Wang, F. Li, B. Li and J.-B. He, *Electrochim. Acta*, 2019, **308**, 285–294.
37 S. Ji, Y. Chen, S. Zhao, W. Chen, L. Shi, Y. Wang, J. Dong, Z. Li, F. Li, C. Chen, Q. Peng, J. Li, D. Wang and Y. Li, *Angew. Chem., Int. Ed.*, 2019, **58**, 4271–4275.
38 A. Goswami, D. Ghosh, V. V. Chernyshev, A. Dey, D. Pradhan and K. Biradha, *ACS Appl. Mater. Interfaces*, 2020, **12**, 33679–33689.
39 M. Jahan, Z. Liu and K. P. Loh, *Adv. Funct. Mater.*, 2013, **23**, 5363–5372.
40 C. A. Downes and S. C. Marinescu, *Dalton Trans.*, 2016, **45**, 19311–19321.
41 R. Dong, Z. Zheng, D. C. Tranca, J. Zhang, N. Chandrasekhar, S. Liu, X. Zhuang, G. Seifert and X. Feng, *Chem.–Eur. J.*, 2017, **23**, 2255–2260.
42 Q. Deng, J. Han, J. Zhao, G. Chen, T. Vegge and H. A. Hansen, *J. Catal.*, 2021, **393**, 140–148.
43 K. Chen, C. A. Downes, E. Schneider, J. D. Goodpaster and S. C. Marinescu, *ACS Appl. Mater. Interfaces*, 2021, **13**, 16384–16395.

44 K. Chen, D. Ray, M. E. Ziebel, C. A. Gaggioli, L. Gagliardi and S. C. Marinescu, *ACS Appl. Mater. Interfaces*, 2021, **13**, 34419–34427.
45 Y.-P. Wu, W. Zhou, J. Zhao, W.-W. Dong, Y.-Q. Lan, D.-S. Li, C. Sun and X. Bu, *Angew. Chem., Int. Ed.*, 2017, **56**, 13001–13005.
46 G. Ruan, P. Ghosh, N. Fridman and G. Maayan, *J. Am. Chem. Soc.*, 2021, **143**, 10614–10623.
47 P. Muthukumar, D. Moon and S. P. Anthony, *CrystEngComm*, 2019, **21**, 6552–6557.
48 P. Muthukumar, M. Pannipara, A. G. Al-Sehemi, D. Moon and S. P. Anthony, *CrystEngComm*, 2020, **22**, 425–429.
49 P. Muthukumar, D. Moon and S. P. Anthony, *Catal. Sci. Technol.*, 2019, **9**, 4347–4354.
50 Q.-F. Chen, Z.-Y. Cheng, R.-Z. Liao and M.-T. Zhang, *J. Am. Chem. Soc.*, 2021, **143**, 19761–19768.
51 D. Fa, J. Yuan, G. Feng, S. Lei and W. Hu, *Angew. Chem., Int. Ed.*, 2023, DOI: **10.1002/anie.202300532**.
52 E. Altin, R. Kirchmaier, A. Lentz and Z. Kristallogr, *New Cryst. Struct.*, 2004, **219**, 137.
53 M. Felloni, A. J. Blake, P. Hubberstey, C. Wilson and M. Schröder, *Cryst. Growth Des.*, 2009, **9**, 4685–4699.